Decay Analysis of ^{197}Tl* Compound Nucleus Formed in ^{16}O + ^{181}Ta Reaction at above Barrier Energy E$_{c.m.}$ ~100 MeV

Gayatri Sarkar[1] (iD), Amandeep Kaur[2] (iD), Manoj K. Sharma[2] (iD) and Moumita Maiti[1*] (iD)

[1]*Department of Physics, Indian Institute of Technology Roorkee, Roorkee, Uttarakhand-247667, India*

[2]*School of Physics and Materials Science, Thapar Institute of Engineering and Technology, Patiala, Punjab-147004, India*

*moumita.maiti@ph.iitr.ac.in (Corresponding Author)

ARTICLE INFORMATION

ABSTRACT

The decay dynamics of ^{197}Tl* compound nucleus has been studied within the framework of the dynamical cluster-decay model (DCM) at above barrier energy E$_{c.m.}$ ≈ 100 MeV using quadrupole deformed configuration of decay fragments. The influence of various nuclear radius parameters on the decay path and mass distributions has been investigated by analysing the fragmentation potential and preformation probability. It is observed that ^{197}Tl* nucleus exhibits the triple-humped mass distribution, independent of nuclear radius choice. The most preferred fission fragments of both fission modes (symmetric and asymmetric) are identified, which lie in the neighborhood of spherical and deformed magic shell closures. Moreover, the modification in the barrier characteristics, such as interaction barrier and interaction radius, is observed with the variation in the radius parameter of decaying fragments and influences the penetrability and fission cross-sections. Finally, the fission cross-sections are calculated for considered choices of nuclear radii, and the results are compared with the available experimental data.

1. Introduction

The nuclear reactions provide useful probe to extract the much-needed information regarding nuclear dynamics. The fusion process in the low-energy region (E<15 MeV/A) allows the investigation of the decay of compound nuclei (CNs) formed in heavy-ion reactions, besides revealing many exciting aspects of nuclear structure and related properties. Thus, the compound nucleus (formed in the excited state) carries high angular momenta and decays by emitting multiple light particles (LPs; *n, p, α*) and γ rays, giving rise to evaporation residue (ERs). Depending upon the mass and energy of the compound nucleus, the emission of intermediate-mass fragments (IMFs) and fusion-fission (FFs) components are also possible. Many theoretical and experimental studies have been carried out to analyze the decay of various light and heavy mass compound nuclei at energies around the Coulomb barrier [1-3]. Recently, the nuclear reaction investigation at energies far above the Coulomb barrier has gain momentum due to advancement in the experimental techniques [4-6] and has opened many interesting questions for exploration at this fermi range physics. Therefore, it is interesting to study a nuclear reaction dynamic at energy much above the Coulomb barrier.

In the present work, the decay dynamics of the ^{197}Tl* nucleus formed in ^{16}O + ^{181}Ta reaction at E$_{c.m.}$=100.88 MeV [1], far above the Coulomb barrier, is carried out by using the dynamical cluster-decay model (DCM) [7-10]. The calculations are performed by incorporating quadrupole (β_{2i}) deformations of the decaying fragments and their optimum orientations $\left(\theta_i^{opt}\right)$ in the hot-compact configuration. The relative impact of different radius vector choices is studied on the compound nucleus decay path by analyzing the fragmentation potential. The behaviour of preformation probability P_0 and scattering potential $V(R)$ is analysed, respectively, to examine the mass distributions and barrier characteristics by opting for different nuclear radii choices. The fusion-fission cross sections $\left(\sigma_{FFs}\right)$ are calculated using the neck-length parameter for all considered radius choices and compared with the experimental data [4].

The manuscript is organized as follows: the description of the theoretical model is presented in Sec. 2, the calculations obtained using DCM are discussed in Sec. 3, and summarized in Sec. 4.

2. Methodology

The DCM [7-10] was developed using the well-known quantum mechanical fragmentation theory (QMFT)

[11, 12], which works in terms of collective coordinates of mass asymmetry $\eta_A = (A_1 - A_2)/(A_1 + A_2)$ (where 1 and 2 stands for heavy and light fragments), relative separation R, the multipole deformations $\beta_{\lambda i} (\lambda = 2,3,4; i = 1,2)$, and orientations $\theta_i (i = 1,2)$. In present work we have confined our calculation to $\lambda = 2$. In terms of these coordinates, the fragment's production cross section for ℓ-partial waves is written as

$$\sigma(A_1, A_2) = \frac{\pi}{k^2} \sum_{\ell=0}^{\ell_{max}} (2\ell+1) P_0 P, \quad k = \sqrt{\frac{2\mu E_{c.m.}}{\hbar^2}} \quad (1)$$

where $\mu = m \left[\frac{A_1 A_2}{A_1 + A_2} \right]$ is the reduced mass. P_o is the fragment's preformation probability and refers to η motion at fixed R value. P is the barrier penetrability and refers to R motion for each η value. Following Eq. (1), the cross sections of FFs processes (i.e., σ_{FF}) are calculated as

$$\sigma_{FF} = \sum_{A_2 = A/2 \pm 20}^{A/2} \sigma(A_1, A_2). \quad (2)$$

The preformation probability P_0 is obtained by solving the Schrödinger equation in η coordinates at fixed R = R_a,

$$\left\{ -\frac{\hbar^2}{2\sqrt{B_{\eta\eta}}} \frac{\partial}{\partial\eta} \frac{1}{\sqrt{B_{\eta\eta}}} \frac{\partial}{\partial\eta} + V(\eta, R, T) \right\} \psi^\nu(\eta) = E^\nu \psi^\nu(\eta),$$

$$(3)$$

with $\nu = 0,1,2,3$, referring to ground state $(\nu = 0)$ and excited state solutions.

The fragmentation potential $\nu(\eta, R, T)$ in the Schrödinger equation (Eq.3) is defined as

$$\begin{aligned} V(\eta, R, T) = & \sum_{i=1}^{2} \left[V_{LDM}(A_i, Z_i, T) \right] \\ & + \sum_{i=1}^{2} \left[\delta U_i \right] \exp\left(-T^2 / T_0^2 \right) \\ & + V_C(R, Z_i, \beta_{\lambda i}, \theta_i, T) \\ & + V_p(R, A_i, \beta_{\lambda i}, \theta_i, T) \\ & + V_\ell(R, A_i, \beta_{\lambda i}, \theta_i, T) \end{aligned} \quad (4)$$

where, V_C, V_P, and V_ℓ are, respectively, the T-dependent Coulomb, nuclear proximity, and centrifugal potentials for deformed and oriented nuclei (for details see Ref. [13]).

The penetration probability P in Eq. (1) is the Wentzel-Kramers-Brillouin (WKB) integral,

$$P = \exp\left[\frac{-2}{\hbar} \int_{R_a}^{R_b} \left\{ 2\mu \left[V(R) - Q_{eff} \right] \right\}^{\frac{1}{2}} dR \right] \quad (5)$$

with $V(R_a, T) = V(R_b, T) = TKE(T) = Q_{eff}(T)$ for the two turning points. The first turning point of the penetration path, R_a, is defined as

$$\begin{aligned} R_a(T) &= R_1(\alpha_1, T) + R_2(\alpha_2, T) + \Delta R(T) \\ &= R_t(\alpha, T) + \Delta R(T), \end{aligned} \quad (6)$$

ΔR is the only adjustable parameter of the model, and is known as the neck-length parameter. The radius vectors $R_i (i = 1,2)$ are obtained as

$$R_i(\alpha_i, T) = R_{0i}(T) \left[1 + \sum_\lambda \beta_{\lambda i} Y_\lambda^{(0)}(\alpha_i) \right], \quad (7)$$

and $R_{0i}(T)$ of the equivalent spherical nuclei is given by

$$R_{0i}(T) = R_{0i}(1 + 0.0007) T^2 \text{ fm.} \quad (8)$$

In the present work, different forms of R_{0i} (whose detailed expressions are given in [14-17]) are considered to study their effect on the decay path of hot and rotated CN. The following expression of different radius vectors are used:

$$R_{0i}^1 = 1.28 A_i^{1/3} - 0.76 + 0.8 A_i^{-\frac{1}{3}} (i = 1,2) \text{fm}, \quad (9)$$

$$R_{0i}^2 = 1.16 A_i^{1/3} - 1.39 A_i^{-1/3} (i = 1,2) \text{fm}, \quad (10)$$

$$R_{0i}^3 = 1.233 A_i^{1/3} - 0.978 A_i^{-\frac{1}{3}} (i = 1,2) \text{fm}, \quad (11)$$

$$R_{0i}^4 = 1.20 A_i^{1/3} - 0.09 (i = 1,2) \text{fm.} \quad (12)$$

3. Calculations and Discussions

DCM calculations are performed using different forms of nuclear radii of the decaying fragments at $E_{c.m.}$=100.88 MeV energy, far above the Coulomb barrier, in reference to the data reported in [1], to understand the decay of ^{197}Tl* compound nucleus formed in ^{16}O + ^{181}Ta reaction.

First, the fragmentation potential $V(\eta, R, T)$ at a common ℓ_{max} is plotted in Fig. 1 to analyse the decay path of CN ^{197}Tl* using four different radii parameters at the best-fitted neck-length parameter (ΔR). It is observed from the figure that the structure of fragmentation potential remains almost identical for all forms of nuclear radii; however, the magnitude of potential is modified significantly. The

Eq. (11) of nuclear radius gives the lowest magnitude and Eq. (9) shows higher values of fragmentation potential as compared to the other forms of nuclear radii.
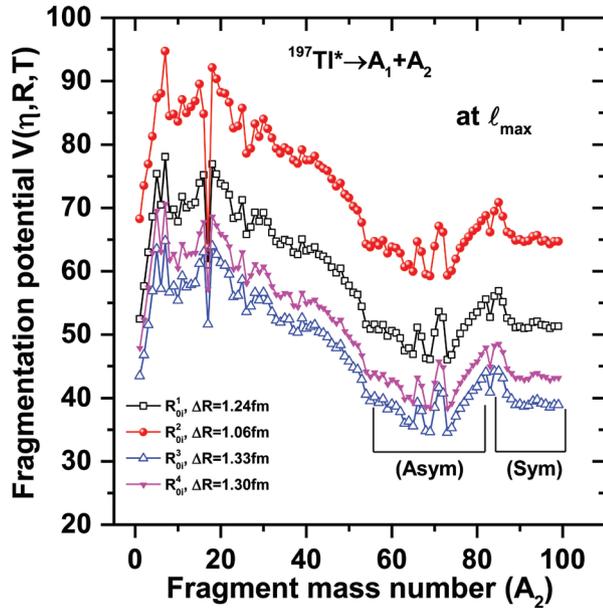
Figure 1: Variation of fragmentation potential with fragment mass number (A_2) using different forms of radius parameters in the decay of $^{197}Tl^*$ at $E_{c.m.}$=100.88 MeV and their corresponding ℓ_{max}.

The fission valleys are also marked in the figure, which corresponds to the symmetric (Sym) and asymmetric (Asym) fission fragments. It indicates the possibility of multi-modal fission of $^{197}Tl^*$ nucleus, i.e., the co-existence of symmetric and asymmetric fission modes. The choice of R_{0i}^3 nuclear radius provides the more energetically favourable fission fragments as compared to other choices. In conclusion, the behaviour of fragmentation potential remains almost same using different forms of radii, i.e., the emergence of ERs, IMFs, and FFs are independent of the choice of radius vectors.

After studying the behaviour of fragmentation potential, the preformation probability P_0 is plotted in Figs. 2a-2d for all choices of nuclear radii (see eqs. (9-12)) at their respective ℓ_{max} for the best-fitted ΔR of fusion-fission cross sections. The fragmentation potential serves as an input to the calculation of preformation probability P_0, the minimum of fragmentation potential corresponds to the maximum of the preformation probability. It is clearly observed from the figure that the $^{197}Tl^*$ compound nucleus shows triple humped mass distribution independent of nuclear radius choice, that means the preformation profile of $^{197}Tl^*$ nucleus suggests the presence of both symmetric and asymmetric fission decay modes simultaneously. The most probable fragments of symmetric and asymmetric fission peaks correspond to ^{99}Nb (Z=41, N=58) + ^{98}Zr (Z=40, N=58) and ^{73}Ga (Z=31, N=42) + ^{124}Sn (Z=50, N=74) decay channels, respectively. Interestingly, these most preferred fission fragments lie in the neighbourhood of spherical (Z=50) and deformed (Z=38, N=60) magic shell closures. Note that the emergence of these fission fragments is independent of nuclear radius choice as marked in Figs. 2a-2d.
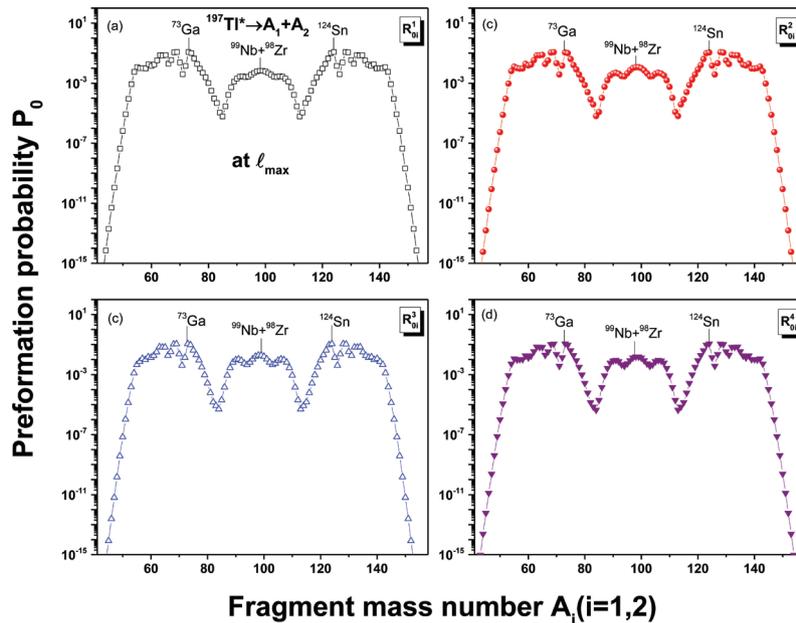
Figure 2: Preformation probability P_0 as a function of fission fragment mass (A_i) for four choices of nuclear radii in the decay of $^{197}Tl^*$ at $E_{c.m.}$=100.88 MeV and their corresponding ℓ_{max}.

For a comparative analysis, the DCM-calculated scattering potential $V(R)$ is shown in Fig. 3 using four different forms of nuclear radii of decay fragments plotted at their respective angular momentum, ℓ_{max}. The barrier characteristics such as interaction barrier height and barrier radius are significantly modified through the different nuclear radii. Consequently, the penetration path of decay fragments gets altered, and hence the penetration probability P changes accordingly. Note that the penetrability P plays a vital role in calculating the decay cross sections. The first turning point (R_a) used in the penetrability calculation is different for various radii of the decay fragments as marked in Fig. 3 and listed in Table 1. This different value of R_a leads to different $V(R_a)$; therefore, the total kinetic energy (TKE) of the fragments also changes with the change in radius. In other words, we can say that the choice of different nuclear radii changes the barrier characteristics, which further influences the CN decay cross sections. Finally, the fission cross sections are calculated within the framework of DCM using all four radius parameters as presented in Table 1 along with the other parameters such as first turning point R_a and best fitted neck-length parameter ΔR. It is observed that each form of nuclear radius parameter is able to address the experimental fission cross sections [1].
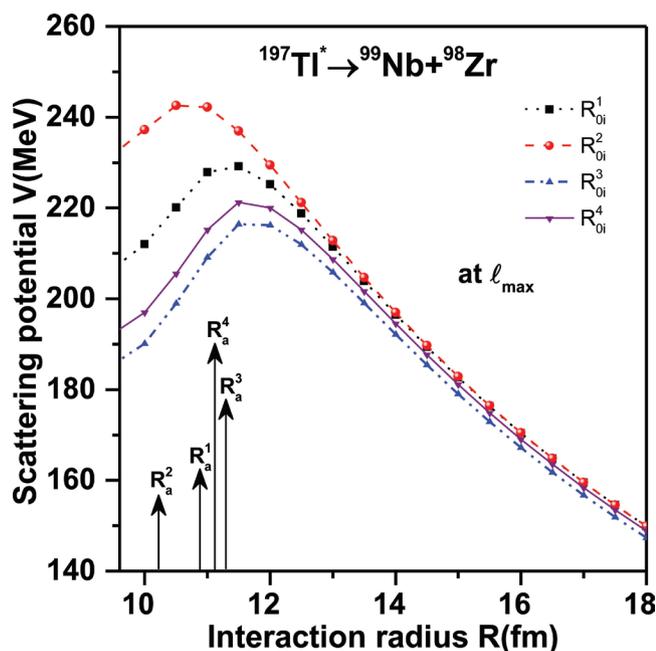
Table 1: The DCM-calculated fusion-fission cross sections using different radii of the decaying fragments at their corresponding first turning point and ΔR values at T=1.89 MeV. Note that the HIVAP-calculated FFs cross section at $E_{c.m.}$=100.88 MeV is 375 mb [1].

Radius (fm)	R_a (fm)	ΔR (fm)	ℓ_{max} (ℏ)	σ_{FFs}^{DCM} (mb)	σ_{FFs}^{HIVAP} (mb)
$R_{0i}^1 (Eq.9)$	10.888	1.24	129	393	
$R_{0i}^2 (Eq.10)$	10.221	1.06	128	392	375
$R_{0i}^3 (Eq.11)$	11.263	1.33	121	370	
$R_{0i}^4 (Eq.12)$	11.178	1.30	126	368	

Summary

Summarizing, we have explored the decay dynamics of ^{197}Tl* compound nucleus formed in ^{16}O+^{181}Ta reaction at energy much higher than Coulomb barrier such as $E_{c.m.} \approx 100$ MeV. All the calculations have been done by employing DCM with quadrupole (β_2) deformed fragments with optimum orientations of hot configurations. Four choices of nuclear radii of decay fragments are considered to analyze the fragmentation potential of ^{197}Tl* compound nucleus. It is observed that the magnitude of fragmentation potential is significantly modified, however, the structure remains almost the same for all forms of radii. The fragmentation potential depicts the co-existence of symmetric and asymmetric fission modes that is further verified via the triple humped mass distribution in preformation probability structure. The identified most probable fission fragments show the relevance of spherical and deformed magic shell closures. It is observed that the choice of different nuclear radius parameters influences the barrier characteristics, and hence the penetrability and decay cross sections get accordingly modified. The fission cross-sections are calculated for different choices of nuclear radii, show decent agreement with experimental data.

Figure 3: DCM-calculated scattering potential V(R) for ^{197}Tl*→^{99}Nb + ^{98}Zr fission channel using different nuclear radii at $E_{c.m.}$=100.88 MeV and for ℓ_{max}.

Acknowledgements

References

[1] D. Kumar and M. Maiti, Physical Review C **96**, 044624 (2017). https://doi.org/10.1103/PhysRevC.96.044624

[2] R. Prajapat and M. Maiti, Physical Review C **101**, 064620 (2020). https://doi.org/10.1103/PhysRevC.101.064620

[3] A. Kaur and M. K. Sharma, Physical Review C **99**, 044611 (2019). https://doi.org/10.1103/PhysRevC.99.044611

[4] P. Jisha et al., Physical Review C **101**, 024611 (2020). https://doi.org/10.1103/PhysRevC.101.024611

[5] C. M. Castaneda, H. A. Smith, Jr., P. P. Singh and H. Karwowski, Physical Review C **21**, 179 (1980). https://doi.org/10.1103/PhysRevC.21.179

[6] A. R. Barnett and J. S. Lilley, Phys. Rev. C **9**, 2010 (1974). https://doi.org/10.1103/PhysRevC.9.2010

[7] R. K. Gupta, M. Balasubramaniam, R. Kumar, N. Singh, M. Manhas and W. Greiner, Journal of Physics G: Nuclear and Particle Physics **31**, 631 (2005). https://doi.org/10.1088/0954-3899/31/7/009

[8] B. B. Singh, M. K. Sharma and R. K. Gupta, Physical Review C **77**, 054613 (2008). https://doi.org/10.1103/PhysRevC.77.054613

[9] M. K. Sharma, S. Kanwar, G. Sawhney, R. K. Gupta and W. Greiner, Journal of Physics G: Nuclear and Particle Physics **38**, 055104 (2011). https://doi.org/10.1088/0954-3899/38/5/055104

[10] M. K. Sharma, G. Sawhney, R. K. Gupta and W. Greiner, Journal of Physics G: Nuclear and Particle Physics **38**, 105101 (2011). https://doi.org/10.1088/0954-3899/38/10/105101

[11] J. Maruhn and W. Greiner, Physical Review Letters **32**, 548 (1974). https://doi.org/10.1103/PhysRevLett.32.548

[12] R. K. Gupta, W. Scheid and W. Greiner, Physical Review Letters **35**, 353 (1975). https://doi.org/10.1103/PhysRevLett.35.353

[13] B. B. Singh, M. K. Sharma and R. K. Gupta, Physical Review C **77**, 054613 (2008). https://journals.aps.org/prc/abstract/10.1103/PhysRevC.77.054613

[14] J. Blocki, J. Randrup, W. J. Swiatecki and C. F. Tsang, Annals of Physics **105**, 427 (1977). https://doi.org/10.1016/0003-4916(77)90249-4

[15] R. Bass, Physical Review Letters **39**, 265 (1977). https://doi.org/10.1103/PhysRevLett.39.265

[16] P. R. Christensen and A. Winther, Physics Letters B **65**, 19 (1976). https://doi.org/10.1016/0370-2693(76)90524-4

[17] A. Winther, Nuclear Physics A **594**, 203 (1995). https://doi.org/10.1016/0375-9474(95)00374-A

Journal of Nuclear Physics, Material Sciences, Radiation and Applications